Off-zone-center or indirect band-gap-like hole transport in heterostructures

Gerhard Klimeck,[1]* R. Chris Bowen,[1] and Timothy B. Boykin[2]
[1]*Jet Propulsion Laboratory, California Institute of Technology, Pasadena, California 91109*
[2]*Department of Electrical and Computer Engineering and LICOS, The University of Alabama in Huntsville, Huntsville, Alabama 35899*

(Received 19 April 2000; revised manuscript received 17 November 2000; published 20 April 2001)

Unintuitive hole transport phenomena through heterostructures are presented. It is shown that for large bias ranges the majority of carriers travel outside the Γ zone center (i.e., more carriers travel through the structure at an angle than straight through). Strong interaction of heavy-, light-, and split-off hole bands due to heterostructure interfaces present in devices such as resonant tunneling diodes, quantum-well photodetectors, and lasers are shown to be the cause. The result is obtained by careful numerical analysis of the hole transport as a function of the transverse momentum k in a resonant tunneling diode within the framework of a $sp3s^*$ second-nearest-neighbor tight-binding model. Three independent mechanisms that generate off-zone-center current flow are explained: (1) nonmonotonic (electronlike) hole dispersion, (2) lighter quantum well than emitter effective masses, and (3) strongly momentum-dependent quantum-well coupling strength due to state anticrossings. Finally a simulation is compared to experimental data to exemplify the importance of a full numerical transverse momentum integration versus a Tsu-Esaki approximation.

DOI: 10.1103/PhysRevB.63.195310 PACS number(s): 73.40.Gk, 72.80.Ey, 71.20.−b, 73.20.At

I. INTRODUCTION

A. Nanoelectronic modeling (NEMO)

The quantum-mechanical functionality of devices such as resonant tunneling diodes (RTD's), quantum-well infrared photodetectors, and quantum-well lasers are enabled by material variations on an atomic scale. The creation of these heterostructure devices is realized in a vast design space of material compositions, layer thicknesses, and doping profiles. The full experimental exploration of this design space is unfeasible and a reliable design tool is needed.

The nanoelectronic modeling tool (NEMO) is one of the first commercial grade attempts for such a modeling tool. NEMO was developed as a general-purpose quantum-mechanics-based one-dimensional (1D) device design and analysis tool from 1993–1997 by the Central Research Laboratory of Texas Instruments (later Raytheon Systems). Free executables can be requested on the NEMO web site.[1] NEMO enables the fundamentally sound inclusion of the required physics: band structure, scattering, and charge self-consistency based on the nonequilibrium Green-function approach. The theory used in NEMO and in this work is documented in Refs. 2–4 while some of the major simulation results are documented in Refs. 5–11. NEMO development is presently continued at the Jet Propulsion Laboratory towards the modeling of light detection and emission devices.

B. Why quantum-mechanical hole transport?

Quantum-mechanical carrier transport research has focused on pure electron transport since most high-speed quantum devices utilize the high-electron mobility in III-V materials. Optical devices, however, typically involve quantum states in the valence bands. We study here the pure hole transport in a hole-doped RTD to begin the study of quantum-mechanical electron and hole transport in laser structures.

C. Approach

Hole states are significantly more complicated than electron states due to the existence of light-hole (LH), heavy-hole (HH) and split-off (SO) bands in (roughly) the same energy range. These bands are coupled[12–15] due to translational symmetry breaking (spatial material and potential variations) that are inherent in any interesting electronic device and due to spin-orbit coupling. Envelope-function representations have been used extensively in much of the published work on hole transport.[16–23] This paper is an extension of previous work by Kiledjian *et al.* who use[24,25] a nearest-neighbor $sp3s^*$ empirical tight-binding basis which includes the spin-orbit interaction to all orders and incorporates wave-function coupling at interfaces through orbital interactions. To better fit[26,27] the complicated valence-band dispersion we include both nearest- and second-nearest-neighbor interactions.[4] The $sp3s^*$ tight-binding parameters used in this work and the corresponding anisotropic masses are published elsewhere.[28] Subband energies and widths are calculated[29] as a function of transverse momentum allowing for an intuitive, yet detailed analysis of hole transport mechanisms.

The work presented here was enabled by the implementation of parallelism[30] in NEMO on simultaneous, various levels: voltage, transverse momentum integration, and energy integration. The use of massively parallel computers enabled the thorough exploration[30] of the state space in total energy E and transverse momentum k for a significant number of bias points.

D. Overview of the paper

Sections II and III discuss approximations for calculating current. Section IV introduces the density of states and the transmission coefficient at zero transverse momentum and identifies and labels the quantized states in the RTD. Section V analyzes the transverse momentum dispersion in the RTD and its effects on the transmission coefficient. Section VI

converts the energy- and momentum-dependent transmission coefficients to a momentum-dependent current density $J(k)$: Failure of the Esaki-Tsu approximation and significant current contributions off zone center are shown. In Sec. VII three origins of the off-zone-center current flow are identified. One of the off-zone-center generating mechanisms is based on the momentum dependence of the resonance widths, which are discussed in more detail in Sec. VIII. Finally a comparison between theory and experiment is examined in Sec. IX and a plea for the simulation of scattering within a multiband basis is made in Sec. X.

II. MOMENTUM-DEPENDENT CURRENT DENSITY $J(k)$

Neglecting scattering in the central RTD region one can compute[2,8,5] the coherent current using an expression of the form

$$J \propto \int dE \int kdkT(E,k)[f_L(E)-f_R(E)] \tag{1}$$

$$= \int dE \int kdkJ(E,k), \tag{2}$$

where k is the electron momentum transverse to the transport direction normalized to the unit cell a by π/a, E is the total energy, T the transmission coefficient, and $f_{L/R}$ the Fermi function in the left/right contact. The dependence on the momentum angle[31] can be shown to be weak.[28]

A transmission coefficient $T(E,k=\text{const})$ as a function of energy may be expensive to compute,[30] since it may contain sharp resonances ($10^{-9}-10^{-3}$ eV) that have to be resolved well in an energy range of typically 1 eV. During the NEMO project algorithms that locate[29] and resolve[32] the resonances expedite the computation of $T(E,k=\text{const})$. The Hamiltonian matrix elements in the device excluding the boundary conditions depend in a nontrivial form on the transverse momentum, while the energy dependence is strictly linear. It is therefore convenient for numerical reasons to reverse the order of integration in Eq. (2), perform the simple Hamiltonian construction as a function of E on the inner loop, and to define an intermediate quantity $J(k)$ as follows:

$$J(k) = \int dEJ(E,k) \tag{3}$$

such that

$$J \propto \int kdkJ(k). \tag{4}$$

For electron transport it can be shown[28] that $J(k)$ typically varies smoothly with k which reduces the number of k points needed to resolve $J(k)$.

This quantity $J(k)$ is not only numerically convenient, but it also bears physical insight as to ''where'' the carrier transport occurs in k space. It can be shown analytically[28] that for an electron RTD the function $J(k)$ is peaked at $k=0$ and monotonically decreasing with k. This behavior indicates that the dominant current contribution arises from carriers at the Brillouin-zone center Γ. For holes, however, it will be shown that $J(k)$ can exhibit sharply peaked features *outside* the Brillouin-zone center Γ ($k_{max}>0$). This indicates that more holes traverse the structure at an angle than straight through the heterointerfaces. This is one of the central results of this paper.

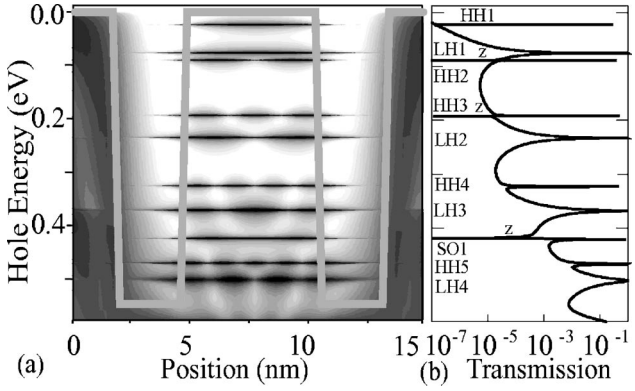

FIG. 1. Density of states (a) and transmission (b) computed in the $sp3s^*$ model. Resonance linewidths are HH1$-$5: 1.4×10^{-5}, 4.5×10^{-4}, 1.8×10^{-3}, 1.2×10^{-2}, 2.8×10^{0} meV; LH1$-$4: 5.4×10^{-2}, 1.7×10^{0}, 4.6×10^{0}, 1.9×10^{1} meV; and SO1: 8.2×10^{-2} meV. Transmission zeros are indicated with *z*.

III. TSU-ESAKI FORMULA

One common approach in reducing the required CPU time[30] needed to compute an I-V characteristic is the assumption of parabolic transverse subbands such that the transmission coefficient has an analytic, parabolic transverse momentum dependence: $T(E,k)=T(E-\hbar^2k^2/2m^*,k=0)$. Under this assumption the transverse momentum integration in Eq. (1) can be carried out analytically to result in the so-called Tsu-Esaki[33] formula,

$$J \propto \rho_{2D} \int dET(E,k=0)\ln\left(\frac{1+e^{(E_F-E)/k\mathcal{T}}}{1+e^{(E_F-E-qV)/k\mathcal{T}}}\right), \tag{5}$$

where $\mathcal{T}$ is the temperature and E_F the Fermi energy in the emitter.

The Tsu-Esaki 1D integration formula is capable of providing qualitatively correct results for electron devices.[34] For hole transport, however, this paper will underline that the analytical Tsu-Esaki integration over the transverse momentum becomes completely invalid.[24,25]

IV. SPECTRAL QUANTITIES: DENSITY OF STATES, TRANSMISSION, AND SUBBANDS

The model RTD considered here consists of ten monolayer (ML) AlAs barriers with a 20 ML GaAs well. To avoid complications due to triangular notch states[5,34] outside the RTD a linear potential drop is applied.[35] A degenerate hole Fermi level of 8.4 meV is assumed corresponding to a doping of 10^{18} cm^{-3}.

Figure 1(a) shows the zero-bias density of states and transmission coefficients computed with the $sp3s^*$ second-nearest-neighbor tight-binding model. The density of states

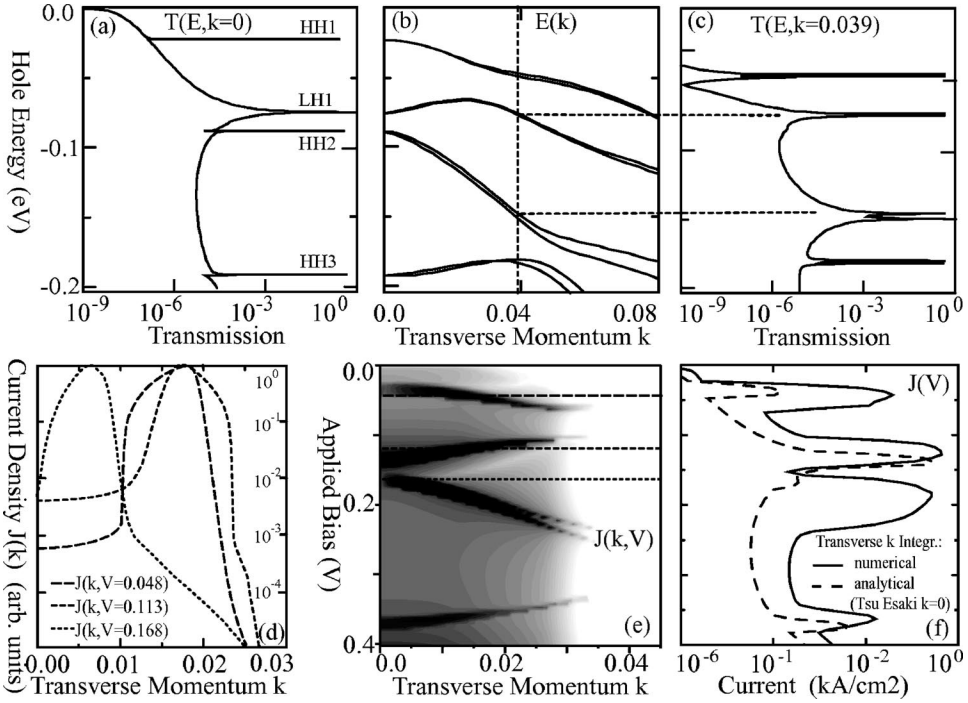

FIG. 2. (a)–(c) Upper panel: Transmission coefficients $T(E,k)$ and transverse momentum dispersion $E(k)$ at zero bias. (a) $T(E,k=0)$ [compare to Fig. 1(b) in a smaller energy range]. (b) $E(k)$, the dispersion is strongly nonparabolic. (c) $T(E,k=0.039)$, transmission is clearly not just an energy-shifted version of the transmission coefficient of (a). Spectral features are significantly altered. (d) Current density integrand $J(k)$ [Eq. (3)] on a logarithmic scale for three different applied voltages: 0.048, 0.113, and 0.168 V. $J(k)$ shows peaks off the zone center at $k>0$. (e) Gray-scale logarithmic plot of the current density integrand $J(k,V)$ as a function of transverse momentum and applied bias (dark=high value, light=low value). The horizontal dashed lines correspond to the three cuts along k shown in (d). (f) Integrated current-voltage characteristics. The solid line indicates complete numerical integration over k. The dashed line is obtained from Tsu-Esaki approximation and therefore corresponds to a vertical cut (Ref. 40) through (e) along the $k=0$ line.

shows the nodal structure of the central RTD resonances. Three sets of nodes, HH1-5, LH1-4, and SO1 can be identified with the increasing number of lobes with increasing hole energy. Each of the resonances corresponds to a peak in the transmission curve [Fig. 1(b)]. The HH mass is significantly larger than the LH mass resulting in a smaller energy separation between the confined states.[36] The barriers are much more opaque for HH than for LH resulting in much stronger confinement.[37] This stronger confinement reveals itself in a significantly smaller resonance width. Indeed the NEMO resonance finder[29] indicates that the LH ground state is over three orders of magnitude wider than the HH ground state as indicated in the caption of Fig. 1.

Note that the transmission coefficient does not reach unity for several of the resonance states due to the coupling of the states even at zero bias. An independent single-band model would provide unity transmission coefficients on resonance.[28] Furthermore, there are some transmission zeros evident in the multiband case[24,21,19] (labeled z in Fig. 1). These features are all characteristics of the Fano line shape that occurs when a bound state is coupled to a continuum.[38] In the case of hole transport *all* the resonances are of the Fano type. Transmission zeros occur for isolated Fano resonances. The zeros move off the real axis in conjugate pairs for overlapped Fano resonances.[29] This explains the lack of transmission zeros for the light-hole resonances. Note that unlike the $\mathbf{k}\cdot\mathbf{p}$ model[21] the $sp3s^*$ model couples the LH, HH, and SO bands for $k=0$ even for zero bias due to symmetry breaking and proper inclusion of the spin-orbit interaction.

V. TRANSVERSE MOMENTUM-DEPENDENT TRANSMISSION COEFFICIENTS

The preceding section discussed the coupled multiband transmission coefficient for zero transverse momentum. The coupling of the bands resulted in nonunity transmission coefficients and Fano resonances. Band anisotropy and band coupling results[25,28] in a rather peculiar transverse energy dispersion. The transverse hole dispersion depends on the details of the resonant tunneling diode such as well and barrier thicknesses. Figure 2(b) shows the hole dispersion for the hole RTD described above at zero bias. Various anticrossings can be traced in the $E(k)$ diagram which serves as more evidence of the interacting quantum states of the various bands. Such strong interaction suggests that there will be a strong dependence of the transmission coefficients on the transverse momentum.[25,28] This strong dependence is demonstrated for two different momenta, $k=0$ and $k=0.039$ in Figs. 2(a) and 2(c), respectively. The location of the resonance energies in Fig. 2(c) corresponds to the intersection of the dispersion in Fig. 2(b) with the dashed vertical line at $k=0.039$. The spin splitting[39] in the dispersion of Fig. 2(c) results in double peaks of the transmission coefficient. Figure

2(c) is not merely an energy-shifted version of the zero transverse momentum case; in fact it has little resemblance at all. The assumption in the Tsu-Esaki formula derivation of $T(E,k)=T(E-\hbar^2k^2/2m^*,k=0)$ breaks down completely for quantized hole states.

The strong transverse momentum dependence in the transmission coefficient shown in Fig. 2(a)–2(c) will result in an interesting dependence of the current flow distribution in momentum and energy as discussed in Sec. VI.

We have also examined the density of states and the structure of the eigenstates at $k=0.039$ corresponding to Fig. 2(c) and found that the nodal symmetries that are visible in the density of states shown in Fig. 1(a) are completely broken. We expect this break in the symmetry to have significant effects on the strength of optical matrix elements and we leave further discussion to a later publication.

VI. CURRENT DENSITY $J(k)$ AND CURRENT-VOLTAGE CHARACTERISTIC

Section V showed a rich structure in the transverse hole dispersion and transmission coefficients. In this section the transmission coefficient $T(E,k)$ is converted into a current density $J(E,k)$ [Eq. (2)] and integrated over energy E [Eq. (3)] to result in the spectral quantity $J(k)$. This integration is performed at a temperature of 4.2 K in a bias range of 0–0.4 V and the resulting spectrum of $J(k,V)$ is plotted in Fig. 2(e) on a logarithmic gray scale. Sharply defined streaks of current flow are visible in the momentum space. The current streaks resemble the transverse subband dispersion if the voltage axis is converted into an energy axis (with a factor of 0.5, due to the linear potential drop). The key information to take from Fig. 2(e) is to realize that the current density $J(k)$ has maxima that are *not* at $k=0$. This is shown explicitly by three cuts through the contour plot at constant voltages of 0.048, 0.113, and 0.168 V in Fig. 2(d). The current density is sharply peaked at a transverse momentum $k\neq 0$ as shown by the logarithmic scale.

Finally, Fig. 2(f) shows two current voltage characteristics computed with[41] [solid line, Eq. (4)] and without [dashed line, Eq. (5)] explicit integration over the transverse momentum on a logarithmic scale. The full integration with the transverse momentum shows a significantly enhanced current flow and current features that do not even show up in the analytic transverse integration. The origin of these additional channels in the current-voltage characteristic is depicted in the plots of the current density $J(k,V)$ of Eq. (3) in Figs. 2(d) and 2(e). The sharp peaks at $k\neq 0$ are completely ignored in the analytical Tsu-Esaki integration that is based solely on the current density at $k=0$. In fact the dashed line in Fig. 2(f) can be considered a vertical cut[40] through the contour of Fig. 2(f) at a constant transverse momentum $k=0$.

Note that the current paths that appear enhanced over the analytical Tsu-Esaki integration appear over wide voltage ranges. One can therefore conclude that the current is dominated by off-zone-center flow in these wide voltage ranges. This conclusion can be verified explicitly using a simple analytical expression for the current.[28] The resonant tunneling diode therefore serves as a nonzero momentum filter. Such a filter might be useful for spin injection systems.

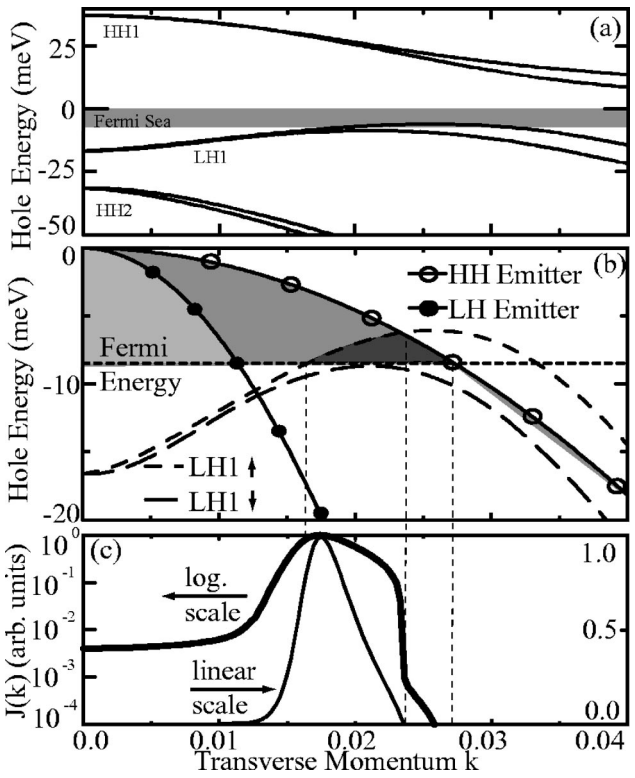

FIG. 3. (a) Transverse dispersion of the HH1, LH1, and HH2 states computed at a bias of 0.113 V (0 meV is the emitter valence-band edge). The gray region indicates the Fermi sea of holes in the emitter. HH1 and HH2 states are out of the energy range for conduction. (b) Detailed plot of (a) in the energy range of transport. LH1↑↓ states (Ref. 39) are shown in dashed lines. The Fermi sea of the emitter is shown as the HH and LH emitter dispersions (lines with symbols) are shown filled (light gray areas) up to the Fermi energy. Dark gray shading shows the momentum and total energy space over which holes in the emitter can find a matching transverse momentum state in the well to tunnel through. (c) Current density $J(k)$ on a linear and logarithmic scale. Current turn-on at $k\approx 0.016$ corresponds to LH1↑ touching into the Fermi sea. Turn-off corresponds to crossing of LH1↑ with the HH emitter band at $k\approx 0.0235$. The linear scale shows that the current is indeed sharply spiked in k.

Figure 2 represents two of the central results of this paper: (1) The current density $J(k)$ can be sharply spiked outside the zone center Γ at $k\neq 0$ indicating that more holes traverse the structure at an angle than straight through, similar to an indirect-band-gap material, and (2) to capture this physics one *must* accurately resolve band structure and perform an explicit numerical integration[41] over the transverse momentum.

VII. ORIGIN OF THE OFF-ZONE-CENTER CURRENT FLOW IN $J(k)$

The previous section demonstrated numerically that there is a significant off-zone-center current flow in hole resonant tunneling diodes for wide voltage ranges. The following

three sections will provide some physical insight into three (almost) independent mechanisms that can generate this unintuitive phenomenon. In Sec. VII A we discuss nonmonotonic dispersion, in Sec. VII B we discuss lighter well than emitter effective mass, and in Sec. VII C we discuss resonance linewidth enhancement at $k>0$.

A. Off-zone-center current flow due to nonmonotonic dispersion

The common understanding of resonant tunneling diode transport for electrons is that the crossing of the bottom of the electron dispersion with the Fermi energy in the emitter starts the current flow in the device. With the strongly nonmonotonic behavior of the hole dispersion [see, for example, the LH1 state in Fig. 2(b) where the dispersion maximum actually occurs at $k=k_{max}>0$] one can imagine that the current turn-on can be determined by the crossing of this maximum of the valence band with the Fermi level. One can therefore expect that most of the current flows in a cone with the momentum k_{max}. Figure 3 verifies this physical argument.

Figure 3(a) provides an overview of the energy scales of the subbands that might be involved in hole transport at a bias of 0.113 V [compare to Fig. 2(b)]. The emitter valence-band edge is set to be the zero-energy origin. The emitter hole states are occupied in a narrow-energy range below the valence-band edge as indicated by the shaded area. The HH1 subband is pulled above the valence-band edge and cannot conduct holes. The HH2 subband is too far below the Fermi sea to conduct. Only the LH1 subband is within reach of the shaded Fermi sea.

Figure 3(b) shows an expanded version of 3(a) in the energy range of the Fermi sea of the emitter. Furthermore, the Fermi sea of the emitter is shown in more detail as the HH and LH emitter dispersions are shown filled (with gray areas) up to the Fermi energy. It is important to note that this is a 3D emitter of holes since we apply no potential drop in the emitter. There is therefore no 2D band quantization in the emitter.

The LH1$\uparrow$ and $\downarrow$ states[39] are shown in dashed lines. At this particular bias it is found that the LH1$\downarrow$ dispersion crosses the Fermi level in a momentum range $k\in[0.016,0.033]$. However, the LH emitter can only provide holes in the range of $k\in[0,0.011]$ and the HH emitter in the range $k\in[0,0.0275]$. There can therefore be no injection of LH states into LH1$\downarrow$ and all the carriers must be injected from the HH emitter states in a momentum range of $k\in[0.016,0.0275]$. The dark gray shade indicates the momentum and energy domain out of which holes one could intuitively expect carriers to be injected into the central resonance states.

Figure 3(c) shows a linear and logarithmic-scale plot of the current density $J(k)$ at the bias of 0.113V. Indeed we find a sharp current turn-on at $k\approx0.016$. However, the first strong turn-off (visible on a logarithmic and linear scale) does not occur at $k\approx0.0275$ but occurs at $k\approx0.0235$. This corresponds to the crossing of the LH1$\uparrow$ dispersion with the HH emitter dispersion. Beyond that crossing the current can

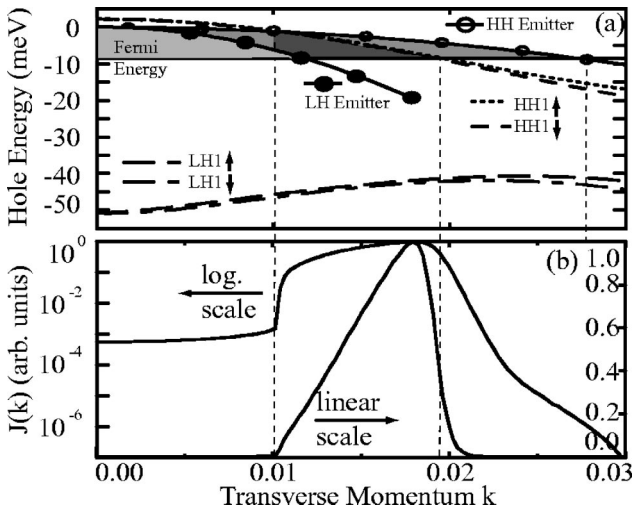

FIG. 4. (a) HH1$\uparrow\downarrow$ and LH1$\uparrow\downarrow$ dispersions at a bias of 0.048V (dashed lines). The Fermi sea of the emitter is shown as the HH and LH emitter dispersions (circles) filled (light gray areas) up to the Fermi level. Crossings of HH1$\uparrow\downarrow$ and HH emitter dispersion with each other and the Fermi level will result in features of $J(k)$ in (b) as indicated by vertical lines. LH emitter states do *not* provide any carriers for injection into the quantum well. (b) Numerical $J(k)$ on a linear and logarithmic scale. Current peak is carried by HH1$\uparrow\downarrow$ states as they pass through the emitter injection dispersion and the Fermi sea.

be shown[28] to be carried by the evanescent quantum state deriving from LH1$\downarrow$ (Lorentzian tail). The final current turn-off at $k\approx0.0275$ of LH1$\downarrow$ is only visible on a logarithmic scale (see dashed vertical lines). No carriers can be provided to the Lorentzian tail of the LH1$\downarrow$ state anymore beyond that point.

Looking at Fig. 3 as a whole one can see how the nonmonotonic behavior of the hole dispersion can create current features that are sharply spiked in the transverse momentum dependence. The following two sections will describe two other mechanisms that can generate similar spikes in $J(k)$.

B. Off-zone-center current flow due a lighter quantum well than emitter effective mass

The previous Sec. VII A showed that quantum state and emitter dispersion crossings at $k>0$ can lead to current turn-ons at $k>0$. Quantum well and emitter dispersion crossings can occur even for simple, almost parabolic, dispersions. In particular, this can occur if the effective mass in the quantum well is significantly smaller than in the emitter as shown in Fig. 4. Similar to Fig. 3 the shape of the current density $J(k)$ is dominated by the crossings of the quantum well dispersions and the emitter dispersion with each other and the Fermi level in the emitter.

At a bias of 0.048V the main current contribution is due to tunneling through the HH1 states as indicated by the dispersions in Fig. 4. The HH1 states have a lighter mass than the bulk HH states due to an admixture of LH components. That can cause a crossing of the dispersions as shown in Fig.

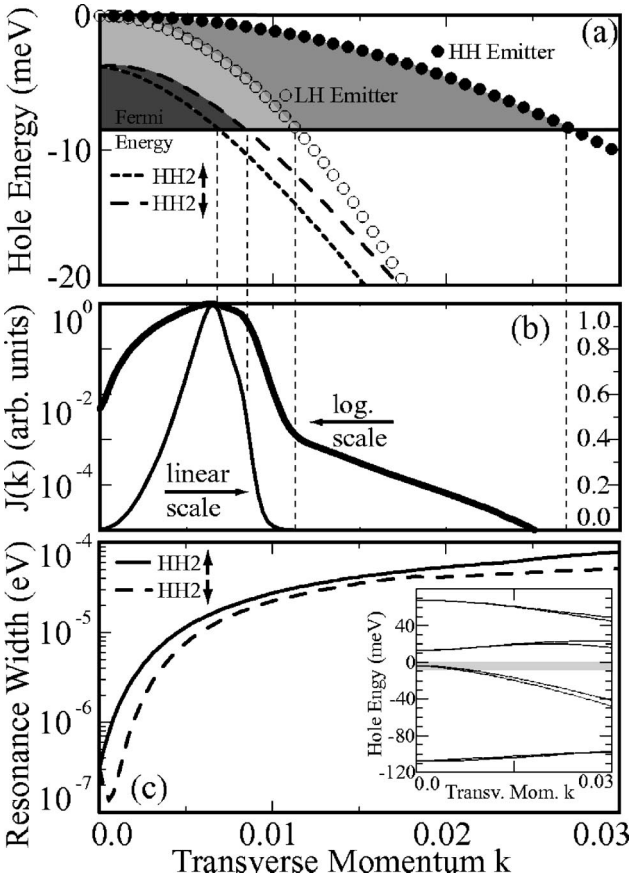

FIG. 5. (a) HH2 dispersion (dashed lines) and HH and LH emitter dispersion (circles) at a bias of 0.168 V. The Fermi sea of the emitter is shown as the HH and LH emitter dispersions are shown filled (with light gray areas) up to the Fermi level in the emitter. Crossings of the dispersions the Fermi level will result in *turn-off* features of $J(k)$ in (b) as indicated by vertical lines. (b) $J(k)$ on a linear and logarithmic scale. The current turn-on is associated with the strong modulation of the resonance width as a function of momentum shown in (c). The inset in (c) is an overview of the quantum-well dispersion at this bias. The gray shade indicates the Fermi sea.

4 at a momentum of $k \approx 0.01$. That crossing corresponds to a turn-on in $J(k)$ in Fig. 4(b). That current turn-on is pronounced on a linear as well as a logarithmic scale. The current turns off at $k \approx 0.019$ when the HH1 dispersion crosses the Fermi sea.

Note that the HH1 has a mass that is lighter than the HH emitter, yet it is still heavier than the LH emitter. The HH1 state and the LH emitter dispersion therefore do not cross. Similar to the case at 0.113 V in Sec. VII A, we assert[28] here again that the current flowing through the structure is dominated by the HH emitter injection at bias of 0.048 V.

It can be shown analytically[28] that the Lorentzian tails of the LH1 states are responsible for the background current of $J(k)$ which finally turns off at $k \approx 0.0275$. To understand this argument one must realize that the HH1 and LH1 states have dramatically different resonance linewidths (see discussions in Sec. VIII).

The phenomenon of crossing quantum well and emitter dispersions is not limited to hole transport, but it is in-

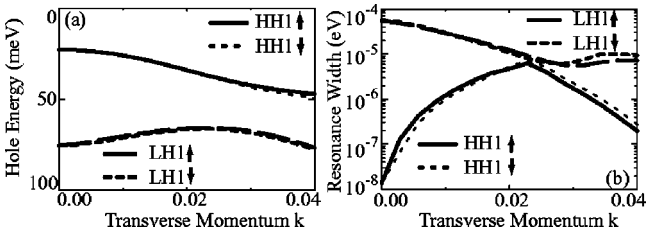

FIG. 6. (a) Same hole dispersion shown in Fig. 2(b) in a smaller energy and momentum range. Only the four lowest energy hole states are shown, including the spin (Ref. 39). (b) Resonance linewidth of the states in (a). The HH1 states show a variation of the resonance linewidth of several orders of magnitude as a function of transverse momentum. The LH1 state shows a reduction of resonance width by about an order of magnitude. The resonances interact very strongly at the anticrossing at $k \approx 0.022$.

deed quite common for high performance InP-based resonant tunneling diodes[42] where the well might contain InAs, while the emitter is typically $In_{0.53}Ga_{0.47}As$ with a larger effective mass.[43,44] We have seen this effect of nonzone-center current flow in direct-band-gap electron devices in such $In_{0.53}Ga_{0.47}As/AlAs/InAs$ high performance RTD systems.

C. Off-zone-center current flow due to resonance linewidth modulations

The preceding two sections VII A and VII B explained how crossings between emitter dispersion, quantum-well dispersion, and emitter Fermi level can lead to current flow that is dominant (sharply peaked) off the zone center in a narrow momentum space. This section will demonstrate how the strong dependence of the resonance linewidth can induce similar off-zone-center current flow.

The inset in Fig. 5(c) shows the dispersion of the lowest eight states at a bias of 0.168 V. The shaded area indicates the width of the Fermi sea in the emitter from which holes can be injected. Only the HH2 states are in the energy range that can provide significant conductance through the structure. Figure 5(a) shows the HH2, HH emitter, and LH emitter dispersions as well as the emitter Fermi level. Given this dispersion one can expect current flow through the HH2 state by injection from either the LH or HH states in the emitter. Current flow is expected to cease as a function of transverse momentum as the quantum well and emitter dispersions are crossing the Fermi sea. Therefore, a monotonically decreasing current density could be expected.[28] However, the resonance widths Γ of the HH2 states show [Fig. 5(c)] an increase by over two orders of magnitude in the transverse momentum range of interest. This increase in Γ leads to a dramatic increase in the current density $J(k)$ as indicated in Fig. 5(b). The following Sec. VIII will examine the origin of the strong resonance linewidth modulation as a function of transverse momentum in a resonant tunneling structure in more detail.

Unlike the preceding two sections where the HH emitter states can be identified as the only current carrying charge injectors one cannot make such an assessment in this case. It

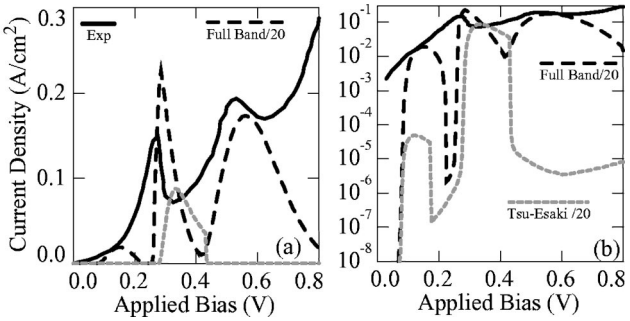

FIG. 7. Current-voltage characteristic (solid line) for an asymmetric hole RTD from Ref. 45 compared to our simulation results with full numerical integration (dashed line) and with analytical (Tsu-Esaki) integration (gray dotted line) scaled down (Ref. 47) by an arbitrary factor of 20.0 (dashed line). (a) Linear scale. (b) Logarithmic scale. The Tsu-Esaki approximation completely misses the third conduction peak similar to Fig. 2(f) and underestimates the first one severely. The deviation between the two simulated results indicates that most of the current flows off-zone center.

can be shown analytically[28] that most of the current is injected from the LH emitter states at this bias.

Note that the turn-on in $J(k)$ appears smoother on a linear scale compared to the previous cases [see Figs. 3(c) and 4(b)]. This is due to the fact that the turn-on is generated by the smooth increase in the resonance linewidth Γ and not by a crossing of the various dispersions with a sharply defined Fermi level at a temperature of 4.2 K.

VIII. RESONANCE LINEWIDTH MODULATION

A. Coupling of HH1 and LH1

Figure 6 sheds light on the interaction of heavy-hole and light-hole states and their coupling to the leads as a function of transverse momentum. Figure 6(a) shows the subband dispersion previously shown in Fig. 2(b) in a smaller energy and transverse momentum range. Only the four top most states including the spins[39] are depicted.

Figure 6(b) shows the associated resonance linewidths[29] as a function of transverse momentum of the first four states. The two highest states (HH1) show the expected (see the caption of Fig. 1) narrow linewidths of about 10^{-8} eV at zero transverse momentum. The next two states have resonance linewidths of about 5×10^{-5} eV which is indicative of the LH states.

Figure 6(a) shows an anticrossing at a transverse momentum of about 0.022. This anticrossing has a very dramatic impact on the heavy-hole coupling to the leads as indicated by the large increase of the resonance linewidth by about three orders of magnitude compared to the zero transverse momentum result. Such a large increase in the resonance linewidth for this particular channel can result in a significant current increase as discussed in Fig. 5 in Sec. VII C. This strong resonance width modulation will only have an impact if there is a significant number of carriers at the transverse momentum of 0.025. This is the case as the Fermi level or the temperature is increased[28] in our RTD. It is emphasized here that the anticrossing has dramatic effects on the resonance linewidths of the involved states over several orders of magnitude, while the resonance state energies are distorted only by a few meV.

B. Coupling between LH1 and HH2

The previous Sec. VIII A illustrated how the HH1 and LH1 state interaction created a significant resonance linewidth modulation at the anticrossing at $k\approx0.022$. Section VII C argued with Fig. 5 that the strong resonance linewidth modulation of HH2 is responsible for the off-zone current flow at a bias of 0.168 V. Here we try to explain this linewidth modulation.

In Fig. 1 the sequence of the lowest hole quantum states in the resonant tunneling diode was identified as HH1, LH1, and HH2 by the nodal symmetry (1, 1, and 2 lobes) in the density of states [Fig. 1(a)] and the widths (narrow, wide, narrow) of the transmission resonances [Fig. 1(b)].

Using Fig. 2(b), however, one can argue that the third state (labeled HH2) has actually the dispersion of a quantized LH state for $k>0$ (large slope). Using a few other diagrams[28] that quantize the anisotropic bulk HH band it can also be shown that the second state labeled here as LH1 has actually HH qualities for $k>0$. It is argued here that there is actually an anticrossing of LH1 and HH2 at $k\approx0$. At $k=0$ the sequence appears to be HH1, LH1, HH2, while for $k>0$ the sequence appears as HH1, HH2, LH1. Correspondingly one can expect the resonance linewidth of the third state to increase significantly with transverse momentum as it changes its character from HH2 to LH1. That is exactly what is shown in Fig. 5(b).

IX. COMPARISON AGAINST EXPERIMENT

Hole resonant tunneling diodes have been investigated experimentally in some detail.[45] Negative differential resistance and effects due to charge accumulation in the central RTD and emitter region have been observed in a variety of different structures.

Hayden *et al.* studied[45] the effect of charge accumulation and intrinsic bistability in an asymmetric RTD. Their structure is described[45] as ''a 4.2-nm GaAs quantum well formed between two AlAs tunnel barriers of thickness 4.5 and 5.7 nm. Undoped spacer layers of thickness 5.1 nm separate the two tunnel barriers from Be-doped contact layers in which the doping is graded from 5×10^{17} cm^{-3} to 2×10^{18} cm^{-3} over a distance of 200 nm.'' The mesa size is assumed[46] to be 100 μm. Figure 7 shows the charge-empty forward-bias direction current-voltage characteristic taken from Fig. 2 of Ref. 45 in a solid line. Without the charge accumulation in the central RTD we can avoid computing the full Hartree charge self-consistently and use a semiclassical potential profile and obtain reasonable[5,8] results.

We entered the structure as described by Hayden[45,46] into NEMO, chose an optical relaxation rate of 24 meV in the contact regions,[5] and used the same second-nearest-neighbor $sp3s^*$ model as in the rest of this paper. In Fig. 7 two simulation results, (1) full numerical transverse momentum integration and (2) analytical transverse momentum integra-

tion, are compared to experimental data. The simulation results have to be scaled down[47] by a factor of 20.0 to be compared to the experimental data on a linear scale.

The main point of this section is not to achieve a perfect fit[47] but it is to highlight the need for a full numerical transverse momentum integration. Similar to the current-voltage characteristic shown in Fig. 2(f) one can see here again that the analytical Tsu-Esaki integration misses a current carrying channel (HH2) completely, and underestimates the channel HH1 significantly.

X. A NEED FOR MULTIBAND-BASIS SIMULATIONS INCLUDING SCATTERING

The comparison in Fig. 7 shows that the simulation is clearly deviating from the experimental results in the valley currents. We attribute this to the lack of incoherent scattering in the central RTD in our simulation. At this stage NEMO can only simulate interface roughness, the polar optical phonon, the acoustic phonon, and alloy disorder scattering in a single-band model.[9–11] Such a single-band model is, however, incapable of incorporating the HH, LH, and SO hole band interactions which are the first-order effects that establish the coherent channels through the central RTD.

For pure electron transport in RTD's it has been shown[9–11] that at low-temperatures band-structure effects are negligible and scattering processes due to optical phonons and interface roughness are dominant. As an overall conclusion to the comparison to experimental data we submit that at low temperatures the combined inclusion of incoherent scattering and the full band structure with full numerical transverse momentum integration is essential to completely model the current flow through a hole RTD.

XI. SUMMARY

This work demonstrates two key findings: (1) HH and LH interaction is shown to be strong enough to result in dominant current flow off the Γ zone center, and (2) proper modeling and explicit inclusion of the transverse momentum in the current integration is needed. Three mechanisms that generate off-zone-center current flow are shown: (1) nonmonotonic (electronlike) hole dispersion, (2) different quantum well and emitter effective masses, and (3) momentum-dependent quantum-well coupling strength. From a comparison of a simulation to experimental data it is suggested that the inclusion of full band structure as well as incoherent scattering is needed to completely model current-voltage characteristics in RTD's.

ACKNOWLEDGMENTS

The work described in this publication was carried out at the Jet Propulsion Laboratory, California Institute of Technology under a contract with the National Aeronautics and Space Administration. The supercomputer used in this investigation was provided by funding from the NASA Offices of Earth Science, Aeronautics, and Space Science. Part of the research reported here was performed using HP SPP-2000 operated by the Center for Advanced Computing Research at Caltech; access to this facility was provided by Caltech. G.K. and R.C.B. would like to acknowledge the careful review of an early manuscript and valuable comments by Marc Cahay. G.K. acknowledges the careful review of the final manuscript by Fabiano Oyafuso.

*Email address: gekco@jpl.nasa.g

[1] See http://hpc.jpl.nasa.gov/PEP/gekco/nemo or search for NEMO on http://www.raytheon.com.
[2] R. Lake, G. Klimeck, R. C. Bowen, and D. Jovanovic, J. Appl. Phys. **81**, 7845 (1997).
[3] R. Lake, G. Klimeck, R. Bowen, D. Jovanovic, and D. Blanks, Phys. Status Solidi B **204**, 354 (1997).
[4] T. B. Boykin, L. J. Gamble, G. Klimeck, and R. C. Bowen, Phys. Rev. B **59**, 7301 (1999).
[5] G. Klimeck, R. Lake, R. C. Bowen, W. R. Frensley, and T. Moise, Appl. Phys. Lett. **67**, 2539 (1995).
[6] R. Lake, G. Klimeck, R. C. Bowen, C. Fernando, D. Jovanovic, D. Blanks, T. S. Moise, Y. C. Kao, M. Leng, and W. R. Frensley, in the *1996 54th Annual Device Research Conference Digest* (IEEE, NJ, 1996), p. 174.
[7] G. Klimeck, T. B. Boykin, R. C. Bowen, R. Lake, D. Blanks, T. S. Moise, Y. C. Kao, and W. R. Frensley, in the *1997 55th Annual Device Research Conference Digest* (IEEE, NJ, 1997), p. 92.
[8] R. C. Bowen, G. Klimeck, R. K. Lake, W. R. Frensley, and T. Moise, J. Appl. Phys. **81**, 3207 (1997).
[9] R. Lake, G. Klimeck, R. C. Bowen, C. Fernando, M. Leng, T. Moise, and Y. C. Kao, Superlattices Microstruct. **20**, 279 (1996).
[10] R. Lake, G. Klimeck, and D. K. Blanks, Semicond. Sci. Technol. **13**, A163 (1998).
[11] G. Klimeck, R. Lake, and D. K. Blanks, Phys. Rev. B **58**, 7279 (1998).
[12] E. E. Mendez, W. I. Wang, B. Ricco, and L. Esaki, Appl. Phys. Lett. **47**, 415 (1985).
[13] R. K. Hayden, D. K. Maude, L. Eaves, E. C. Valadares, M. Henini, F. W. Sheard, O. H. Hughes, J. C. Portal, and L. Cury, Phys. Rev. Lett. **66**, 1749 (1991).
[14] J. A. Kash, M. Zachau, M. A. Tischler, and U. Ekenberg, Phys. Rev. Lett. **69**, 2260 (1992).
[15] W.-C. Tan, J. C. Inkson, and G. P. Srivastava, Phys. Rev. B **54**, 14 623 (1996).
[16] J. M. Luttinger and W. Kohn, Phys. Rev. **97**, 869 (1955).
[17] M. Burt, Semicond. Sci. Technol. **3**, 739 (1988).
[18] B. Foreman, Phys. Rev. Lett. **81**, 425 (1998).
[19] S. Ekbote, M. Cahay, and K. Roenker, Phys. Rev. B **58**, 16 315 (1998).
[20] S. Ekbote, M. Cahay, and K. Roenker, J. Appl. Phys. **87**, 1467 (2000).
[21] C. Y.-P. Chao and S. L. Chuang, Phys. Rev. B **43**, 7027 (1991).
[22] Y. X. Liu, R. R. Marquardt, D. Z.-Y. Ting, and T. C. McGill, Phys. Rev. B **55**, 7073 (1991).
[23] J. X. Zhu, Z. D. Wang, and C. D. Gong, Solid State Commun. **101**, 257 (1997).
[24] M. S. Kiledjian, J. N. Schulman, K. L. Wang, and K. V. Rous-

seau, Phys. Rev. B **46**, 16 012 (1992).
[25] M. S. Kiledjian, J. N. Schulman, K. L. Wang, and K. V. Rousseau, Surf. Sci. **267**, 405 (1992).
[26] G. Klimeck, R. C. Bowen, T. B. Boykin, C. Salazar-Lazaro, T. A. Cwik, and A. Stoica, Superlattices Microstruct. **27**, 77 (2000).
[27] G. Klimeck, R. C. Bowen, T. B. Boykin, and T. A. Cwik, Superlattices Microstruct. **27**, 519 (2000).
[28] Gerhard Klimeck, R. Chris Bowen, and Timothy B. Boykin, Superlattices Microstruct. **29**, 187 (2001).
[29] R. C. Bowen, W. R. Frensley, G. Klimeck, and R. K. Lake, Phys. Rev. B **52**, 2754 (1995).
[30] For the simulations presented in this work parallelization was utilized in the integration over the independent momenta *k*. Typically 150 points were used for the momentum resolution, while the energy grid resolution may vary adaptively from a few hundred nodes to several thousand nodes depending on the number of resonances in the energy range of interest. The load on 16 or 32 CPU's was balanced in a master-slave approach due to the variability in the execution time of each energy integration. The simulations were run on a 32 CPU Beowulf system based on 450-MHz Pentium III, on a SGI Origin 2000, and HP SPP-2000. The final runs that resolve several hundred bias points took about a week to run on our dedicated Beowulf system. The Tsu-Esaki formula [Eq. (5)] is so tempting to be used since it reduces the required CPU time in this case by a factor of 150. A more fine-grain parallel integration over energy *E* or a more coarse-grain parallelism over bias points can be used in NEMO for such a computation where there is no explicit integration over momentum *k*.
[31] In this work we assume cylindrical symmetry and use the transverse momentum in the [100] direction.
[32] G. Klimeck, R. Lake, R. C. Bowen, C. L. Fernando, and W. R. Frensley, *Resolution of Resonances in a General Purpose Quantum Device Simulator* (NEMO) (Gordon and Breach, New York, 1998), Vol. 6, p. 107.
[33] R. Tsu and L. Esaki, Appl. Phys. Lett. **22**, 562 (1973).
[34] The Tsu-Esaki can provide qualitatively correct results for electron devices given the restrictive assumption that subband alignment is *not* the primary transport mechanism (Refs. 48–50,8). Technologically relevant RTD's that show negative differential resistance at room temperature all exhibit a triangular emitter well such that there is a large 2D to 2D subband tunneling contribution from emitter to central resonance. To achieve quantitative agreement (Refs. 7 and 8) between simulation and experimental data for such RTD's full 2D integrations in energy *E* and transverse momentum *k* according to Eq. (2) must be performed.
[35] There is no implicit limitation in NEMO to a linear potential drop. Charge self-consistent simulations of the Hartree and exchange and correlation potential are presented in Refs. 5, 7, and 8.
[36] In an infinite barrier square well of width *a* the energy separation is $\Delta E_{n+1}=E_{n+1}-E_n \propto \hbar^2\pi^2/2ma^2 \propto 1/m$.
[37] For a single square barrier of thickness *d* the exponential $e^{-\kappa d}$ decay constant is defined as $\kappa=\sqrt{2m\Delta E/\hbar^2}\propto\sqrt{m}$.
[38] U. Fano, Phys. Rev. **124**, 1866 (1961).
[39] The asymmetry of the applied bias has split the two spin states. Note that there is no magnetic-field selection in these simulations. The spin-degenerate states at $k=0$ are split due to the translational symmetry breaking at $k>0$. We use the notation $\uparrow,\downarrow$ as a shorthand to identify the two states. Since there is no selecting magnetic field we assume that, for example, LH1$\uparrow$ consists of a linear combination of up and down spins.
[40] $J(k=0)$ scales directly with the total current if the Tsu-Esaki formula is employed [Eq. (5)] except for a scaling factor including the 2D density of states ρ_{2D}.
[41] We find good numerical stability in these hole RTD's when about 150 *k* points are resolving a uniform *k* grid in the range of 0–0.05. This number of *k* points could possibly reduce if an adaptive *k* grid were to be introduced.
[42] T. S. Moise, Y.-C. Kao, A. J. Katz, T. P. E. Broekaert, and F. G. Celii, J. Appl. Phys. **78**, 6305 (1995).
[43] T. B. Boykin, Phys. Rev. B **51**, 4289 (1995).
[44] J. N. Schulman, Appl. Phys. Lett. **72**, 2829 (1998).
[45] R. K. Hayden, L. Eaves, M. Henini, D. K. Maude, and J. C. Portal, Phys. Rev. B **49**, 10 745 (1994).
[46] R. K. Hayden (private communication). The mesa sizes used in the experiment have diameter of 100 μm.
[47] While a deviation by a factor of 20 might sound large we point out here that such a deviation is not completely unexpected. We have verified with NEMO that variations of 2–3 monolayers in the barrier thickness and variations in the doping profile detail can result can result in such current density variations of factors of 20. We feel that such deviations can only be eliminated in a controlled test matrix (Ref. 7) of experimental structures where experimental trends can be analyzed in more detail. Such a controlled comparison between experiment and theory or arbitrary adjustments to parameters until a perfect fit is achieved are not the point of this presentation.
[48] T. B. Boykin, R. E. Carnahan, and R. J. Higgins, Phys. Rev. B **48**, 14 232 (1993).
[49] T. B. Boykin, R. E. Carnahan, and K. P. Martin, Phys. Rev. B **51**, 2273 (1995).
[50] T. B. Boykin, J. Appl. Phys. **78**, 6818 (1995).